

Outline

Contents

1	Introduction	2
2	Methods	3
2.1	Model description	3
2.2	Large ensemble	4
2.3	Data	6
3	Results I: Historical evolution of the Southern Ocean carbon sink	7
4	Results II: Spatial distribution of Southern Ocean carbon sink	9
4.1	Negative trends in carbon sink	11
4.1.1	Changes in biology in negative trends	12
4.1.2	Changes in ocean circulation in negative trends	14
4.2	Positive trends in carbon sink	15
4.2.1	Changes in biology in positive trends	17
4.2.2	Changes in ocean circulation in positive trends	19
4.3	Internal Variability due to winds	20
5	Discussion	21
6	Summary and conclusions	22

1 Introduction

why Southern Ocean is important carbon budget oceanic uptake [Sabine et al., 2004] [Le Quéré et al., 2016] outcrop area [Marshall and Speer, 2012] SO as constraint to reduce model uncertainties [?]

Southern Ocean observations and call for models Observation-based estimates report a large variability in the Southern Ocean carbon sink [Le Quéré et al., 2007, Landschützer et al., 2015]. Sparse observational data lack the ability to show the dynamics of internally varying processes, which demands for the evaluation with models.

Hypothesis The Southern Annular Mode (SAM), characterizing the strength and position of the westerly winds, is known to be the dominant mode of climate variability in the Southern hemisphere. Supposing the strength of the westerlies winds as the major reason for climate variability for the Southern Ocean, how does the carbon system respond? Strengthening westerlies increase upwelling, so more carbon-rich waters entrain the upper ocean and hence outgas. This upwelling also brings additional nutrients for the deep ocean, which might foster primary production. However, if the wind mixes too strong though, primary production decreases because of light limitation [Sverdrup, 1953].

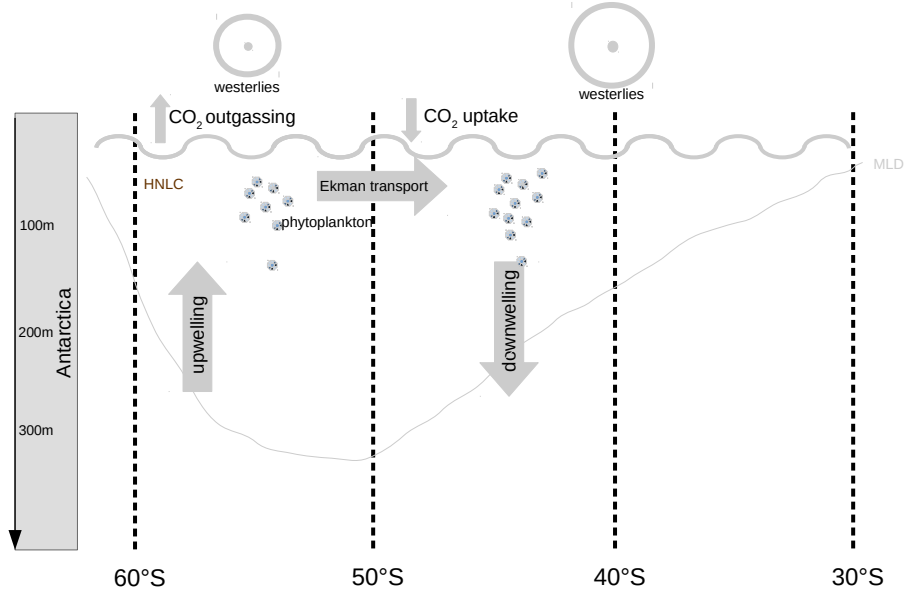


Figure 1: Schematic illustration of the Southern Ocean ; probably wrong location here, but where to put it? Results I after the mean state results?

Previous studies on mechanism and trends, modelling and observations Previous modeling studies were studying the impact of SAM on the carbon sink [Lovenduski

et al., 2007, Hauck et al., 2013] or long-term carbon trends [Wang and Moore, 2012] using ocean-only models with atmospheric historic forcing. biology response on SAM [Lovenduski and Gruber, 2005]

What I do and research questions By using a large ensemble simulation based on the Max-Planck-Institute Earth System Model (MPI-ESM), I investigate the variability of the oceanic carbon uptake. I try to answer the following questions: How large is the internal variability of the Southern Ocean carbon sink? Are large ensembles able to reproduce decreasing decadal trends of the Southern Ocean carbon sink? How does variability in physical processes influence biology and hence the carbon sink?

2 Methods

2.1 Model description

listing MPI-ESM components The MPI-ESM version 1.1 with a low-resolution configuration (MPI-ESM-LR) is used for the large ensemble simulations [Giorgetta et al., 2013]. The atmosphere component ECHAM6.3 runs on a T63 grid, corresponding to 1.9° horizontal resolution, with 47 vertical layers up to 0.01 hPa [Stevens et al., 2013]. Atmospheric pCO₂ levels are prescribed due to the CMIP5 protocol and well mixed [Taylor et al., 2012]. The carbon cycle is not coupled, so called diagnostic, so effects of changes in the terrestrial or oceanic carbon sink are not reflected in the atmospheric pCO_{2,atm}. Since there is no biogeochemical riverine exchange, terrestrial and oceanic carbon sink do not interact (Fig. 2). The ocean component MPI Ocean Model (MPIOM) has a horizontal resolution of 1.5° on average and 40 vertical levels [Jungclaus et al., 2013]. The Hamburg Ocean Carbon Cycle Model (HAMOCC) represents the ocean biogeochemistry component and aims to describe the carbon cycle (Fig. 3) [Ilyina et al., 2013].

basics in HAMOCC - needed ? HAMOCC is coupled to the atmospheric component ECHAM6 to exchange carbon dioxide (CO₂), oxygen (O₂), nitrogen (N₂), nitrous oxid (N₂O), and dimethyl sulfide (DMS) with the top layer of the euphotic zone. Iron enters the water column via dust input climatology. The required state variables required for HAMOCC, e.g. sea-ice cover, temperature T, salinity S and advective velocities \vec{v} , are provided from MPIOM. Most tracers get advected by the flow field and can get diluted by freshwater or mixing. The chemistry in HAMOCC is modeled in the carbonate system and keeps track of alkalinity.

In the euphotic zone upto a depth of 90m, primary production can convert nutrients, e.g. phosphate (PO₄), nitrate (NO₃), and iron, and inorganic carbon to organic matter by photosynthesis. The predator-prey relationship in HAMOCC follows a NPZD model [Six and Maier-Reimer, 1996]. Phytoplankton proliferate from nutrient consumption, zoo-

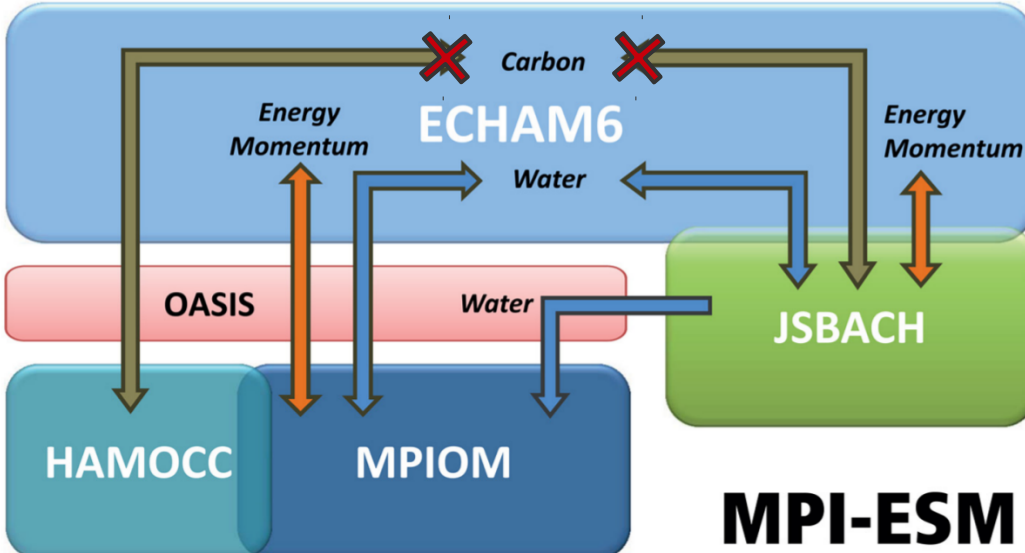


Figure 2: Schematic overview on the different components in MPI-Earth-System-Model with a diagnostic carbon cycle [Giorgetta et al., 2013]

plankton from phytoplankton consumption while detritus is left over as dead particulate organic material. While detritus sinks to the ocean floor, it partly remineralizes. There are two fractions of detritus: opal producing if silicate is available or calcium carbonate producing. Calcification then changes the alkalinity and carbon budget.

Primary production is parametrized by bulk phytoplankton which mimics diatom's, coccolithophore's and dinoflagellate's combined growth under exponentially increasing optimum growth rate temperatures [Eppley, 1972]. Phytoplankton and zooplankton belong to the pool of organic carbon.

At the ocean floor, all tracers are in exchange with the sediment which included pore water exchange processes and accumulation of particulate matter in the burial layer [Heinze et al., 1991].

2.2 Large ensemble

general: what is it? how produced technically? Large ensemble simulation are a novel tool to investigate internal variability. By repeating a climate simulation with an identical forcing and model code but changing the initial conditions slightly, single ensemble members will be exposed to the same process implementations but the interplay are at a stochastically random level lets each realisation evolve in a unique way while still being bound to a common forced trend.

The MPI-ESM Large Ensemble (MPI-ESM LE) contains 100 simulations under historical CMIP5 forcing from 1850 to 2005 and is extended under Representative Concentration

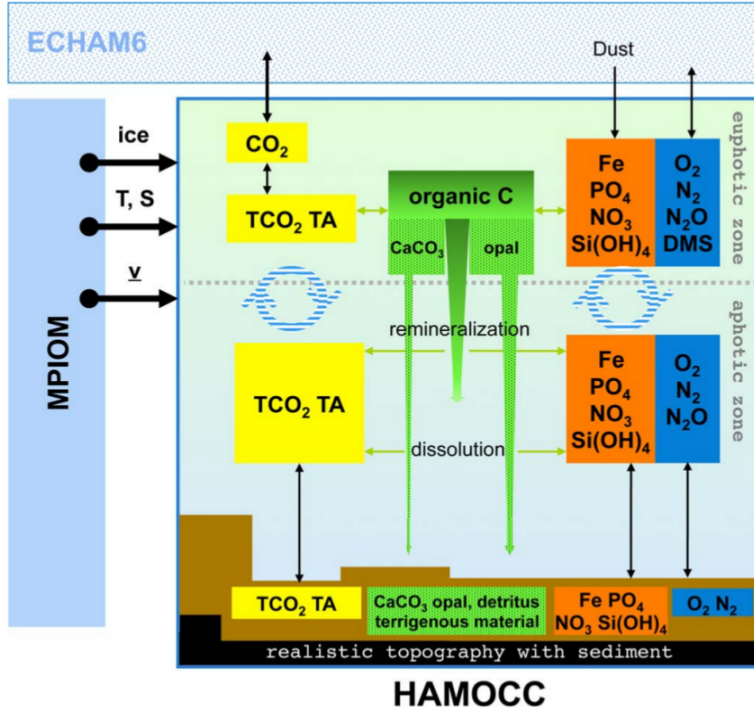


Figure 3: A schematic overview of the global ocean biogeochemistry model HAMOCC [Ilyina et al., 2013]

Pathway (RCP) 4.5 scenario until 2100. Ensemble members differ through starting from different year of the pre-industrial control simulation, so ocean and atmosphere have different initial conditions in each run. This was achieved by branching off ensemble members from the control run after roughly 50 years by increasing the atmospheric pCO_2 levels.

MPI-ESM LE data already provided data to a few MPI-M publications, e.g. [Marotzke and Forster, 2015, Bittner et al., 2016].

novel method: how are other ensembles different? As large ensemble research is a recent feature due to powerful upscaling of super-computing facilities, the number of ensemble datasets is limited and published papers infrequent.

NCAR's Community Earth System Model large ensemble (CESM LE) [Kay et al., 2015] underlies the pioneering internal variability studies of Deser et al.. The initial state of the atmosphere was slightly perturbed by roundoff-level changes to air temperature in their 32 runs. CESM LE served for studies analyzing the timescales of detection of trend in the ocean carbon sink [McKinley et al., 2016] and the partitioning of its uncertainties [Lovenduski et al., 2016].

GFDL ran a 30-member ensemble simulation based on their model ESM2M. They use different dates separated by one day each but didn't publish any oceanic carbon uptake

paper [Rodgers et al., 2015].

Previous studies assume gaussian statistics, but lack an adequate ensemble size to check for in detail [Thompson et al., 2015, Deser et al., 2012].

2.3 Data

where are they from and why I choose this product? For comparison of CO₂flux with model simulations, I use the SOM-FFN data which is based on the Surface Ocean Atlas Version 2 (SOCATv2) [Landschtzer et al., 2016]. It uses a neural network-based data interpolation to create pCO₂ maps [Landschtzer et al., 2014]. I use this pCO₂ data product because it seems a smart interpolation of pCO₂ data to cover regions without direct pCO₂ measurements. However, the input training data of the algorithm is heavily seasonally biased, as the available pCO₂ samples originate mostly from austral summer months.

3 Results I: Historical evolution of the Southern Ocean carbon sink

carbon sink SO: forced trend and int variability, int var results explain fig. 4; Internal variability, defined as the σ -spread of the 100-members, is constant over this period ($0.18 \pm 0.02 \text{ PgC yr}^{-1}$).

comparison ensemble to data SOM-FFN data ranges within the 2σ ensemble spread. We find carbon trends similar to those in the 1990s and 2000s.

choice of trends: compromise signal strength and signal length monotonic compromise between decade=10yrs vs interannual variability, not too strong influence of atmospheric forced trend and strength of signal Fig 22; Exemplary for all decadal carbon sink trend ensemble members, I show the most extreme cases. The underlying mechanisms for carbon sink trends in our ensemble simulation seem to be of the same origin.

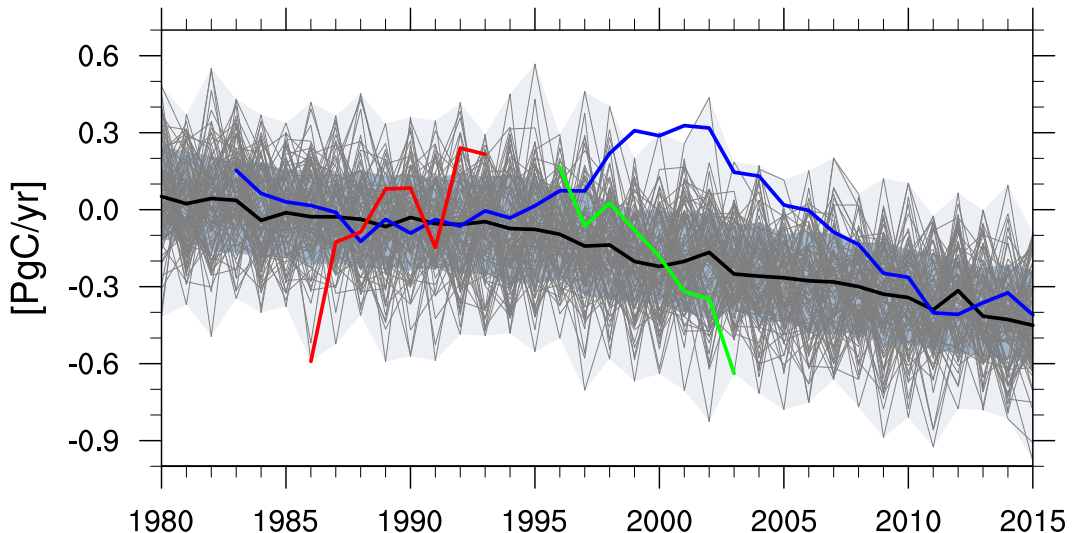


Figure 4: Evolution of the Southern Ocean carbon sink anomaly south of 35°S . Grey lines show the 100 ensemble members, the black line the ensemble median, the gray shading is the range of the ensemble, the blue shading is the 1σ ensemble spread, the red lines are decreasing sink trend candidates, the blue line is the SOM-FFN observation-based estimate; negative values indicate anomalous uptake with respect to the 1980s

timeseries sam, biology, upwelling index? nice-to-have, but no connection to storyline; results I: seems short

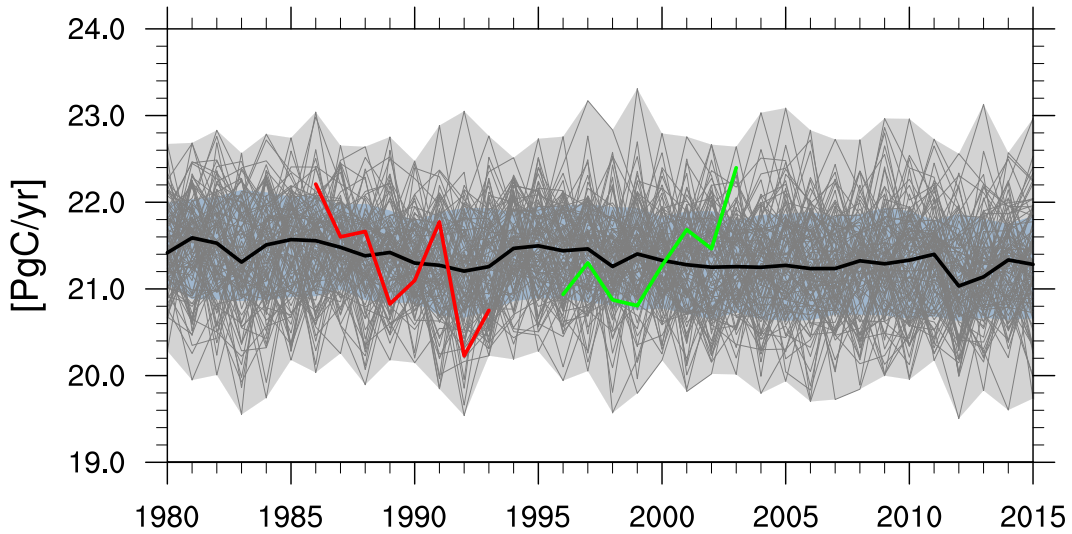


Figure 5: Evolution of the Southern Ocean primary production south of 35°S . Grey lines show the 100 ensemble members, the black line the ensemble median, the gray shading is the range of the ensemble, the blue shading is the 2σ ensemble spread, the red lines are decreasing sink trend candidates

transition to process understanding in spatial view; afterwards only two members shown exemplarily As shown in previous studies [Le Quéré et al., 2007], the variations of oceanic carbon uptake are related to the background thermal and dynamic changes. Some note on biology

4 Results II: Spatial distribution of Southern Ocean carbon sink

mean state and internal variability Southern ocean carbon sink refer to fig. 6

mean state and internal variability Southern ocean westerly winds? no plot yet

mean state and internal variability of biology and link to carbon sink refer to fig. 6

mean state and internal variability of upper ocean circulation and link to carbon sink refer to fig. 7

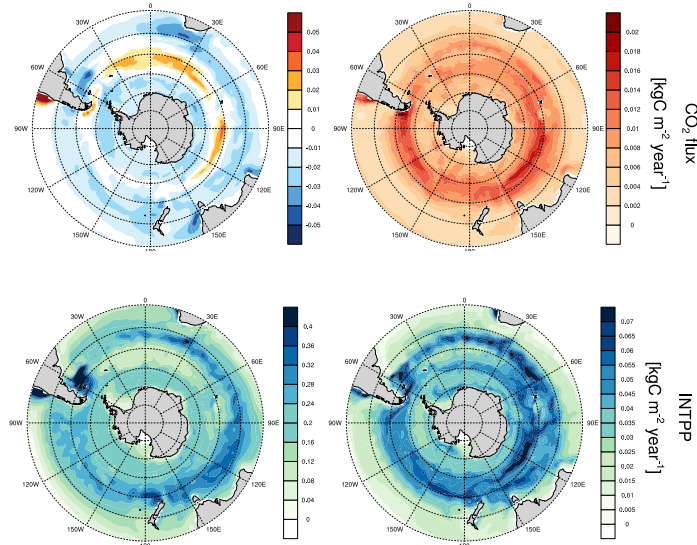


Figure 6: Spatial distribution of the yearmean Southern Ocean CO₂flux (top) and primary production (bottom): negative values indicate ocean uptake ensemble median (left) as forced signal and ensemble standard deviation (right) as internal variability

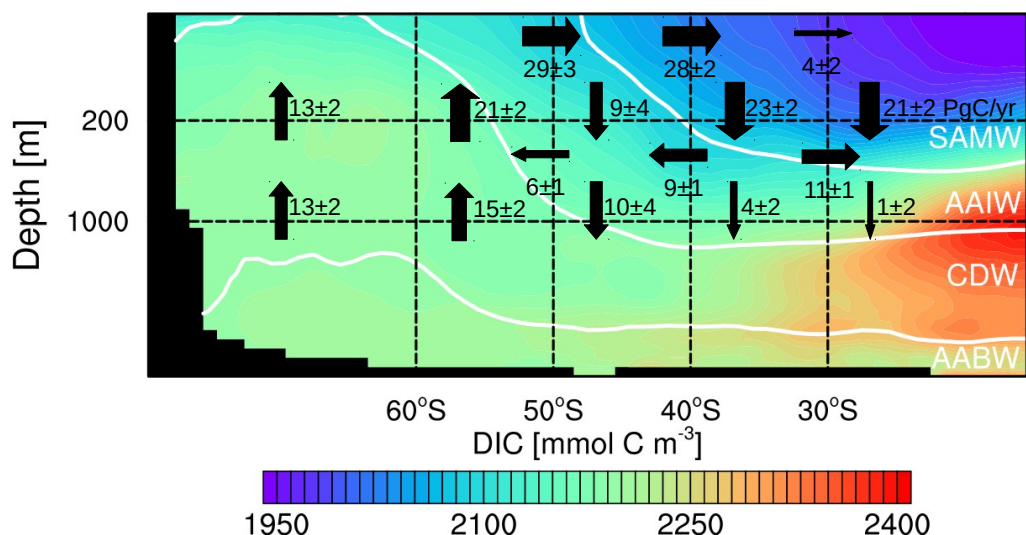


Figure 7: Upper-ocean overturning circulation modulates the carbon sink as carbon-rich water are upwelled and carbon-depleted water are downwelled; black arrows show yearly mean advective carbon transport; white lines are isopycnals separating Sub-Antarctic Mode Water (SAMW), Antarctic Intermediate Water (AAIW), Circumpolar Deep Water (CDW) and Antarctic Bottom Water (AABW)

4.1 Negative trends in carbon sink

trends in pCO₂ and westerly winds refer fig. 8 pCO₂ and not co2flux to show co2flux not only increasing due to stronger winds in $\text{co2flux} = (1 - f)\text{wind}^2 * \text{Sc}(T)/600 * dp\text{CO}_2$ [Wanninkhof, 1992] The region of 50-60°S has the strongest decreasing trend in CO₂flux. leads to hypothesis

schematics: explain carbon decrease due to wind refer to fig. 9 - can I show this already here or better after the plots

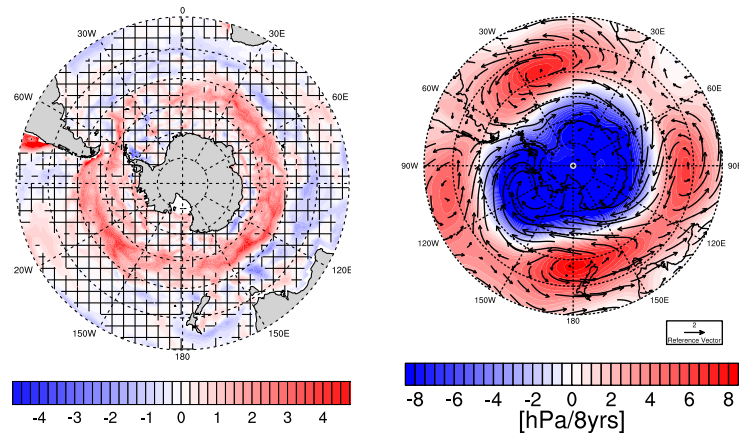


Figure 8: pCO₂(right) (left) and Trends in sea-level pressure and winds

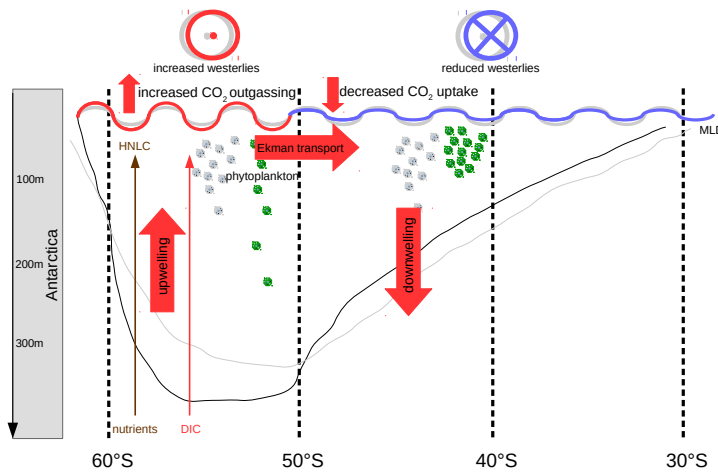


Figure 9: Schematic illustration of the Southern Ocean under the context of increasing westerly winds and response of biology and upper-ocean circulation towards the carbon sink

4.1.1 Changes in biology in negative trends

on trends in co2flux, intpp Primary production and CO₂flux show opposing trend patterns as plankton growth takes up large amounts of surface DIC and hence lowers pCO₂

on explaining intpp decrease in 50s: using zmld mixing

on intpp not increasing because of more nutrients different than [Lovenduski and Gruber, 2005] (can I cite this here or only in discussion?)

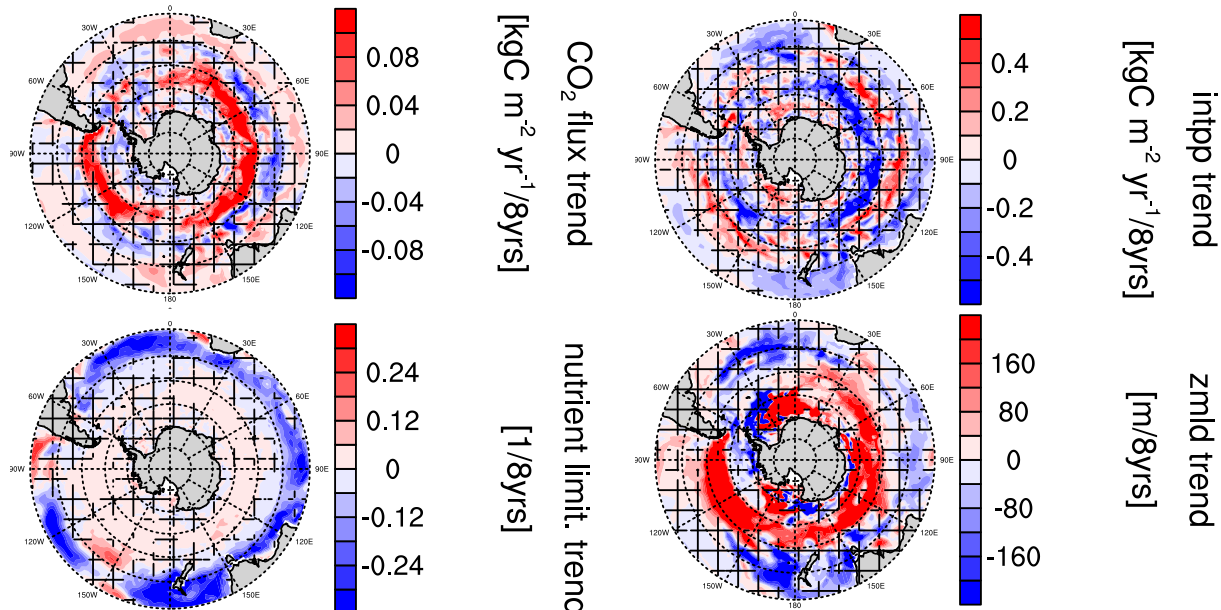


Figure 10: Southern Ocean austral summer trends per per 8 years

on mixing, sverdrup as cause for intpp decrease Sverdrup [Sverdrup, 1953] introduced his concept of critical depth based turbulent mixing as a requirement for plankton blooms [Franks, 2014]

balance of mass of phytoplankton and wind penetration depth refer fig. 11

concentration increase of intpp at 40s due to advection/ekman transport refer fig. 12

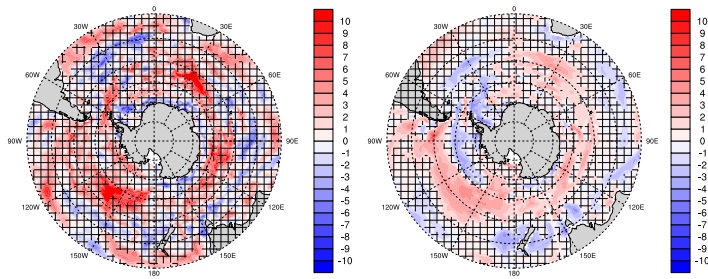


Figure 11: Trends in [m/8yrs] for phytoplankton average depth (left) and average depth of vertical diffusivity due to wind (right); hatched areas indicate where trends were below 5% significance

4.1.2 Changes in ocean circulation in negative trends

transition: zmlt trends; Upper-ocean overturning circulation: up, ekman transport, downwelling The strong trend in MLD could also be a sign of increasing outgassing due to more mixing (fig. 10). refer to fig. 12

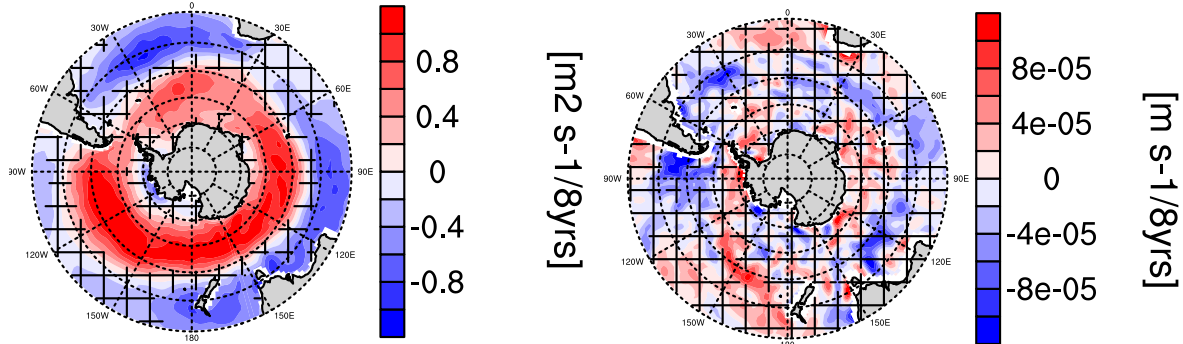


Figure 12: Ekman transport and ekman upwelling trends

carbon transport changes refer fig. 13

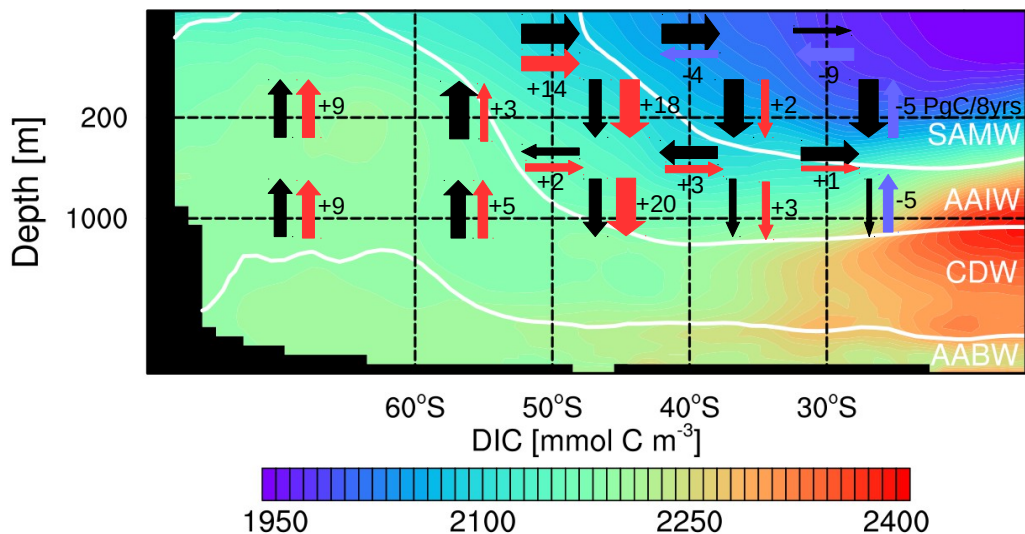


Figure 13: Increased upper-ocean overturning circulation weakens the carbon sink as carbon-rich water are upwelled and carbon-depleted water are downwelled

4.2 Positive trends in carbon sink

disclaimer: everything upside down

trends in pCO₂ and westerly winds refer fig. 14 The region of 50-60°S has the strongest decreasing trend in CO₂flux. leads to hypothesis

schematic changes due to wind refer to fig. 15

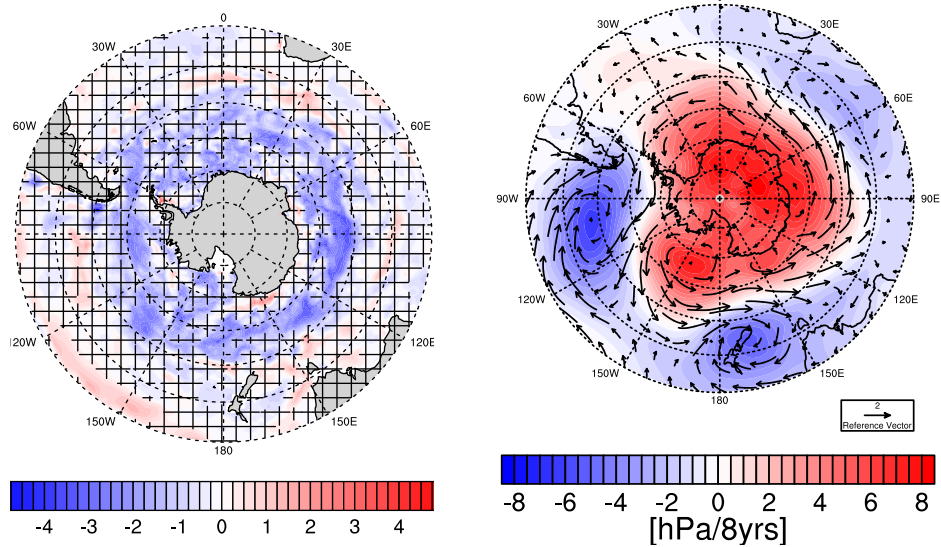


Figure 14: Trends in pCO₂ (left) and sea-level pressure and winds (right)

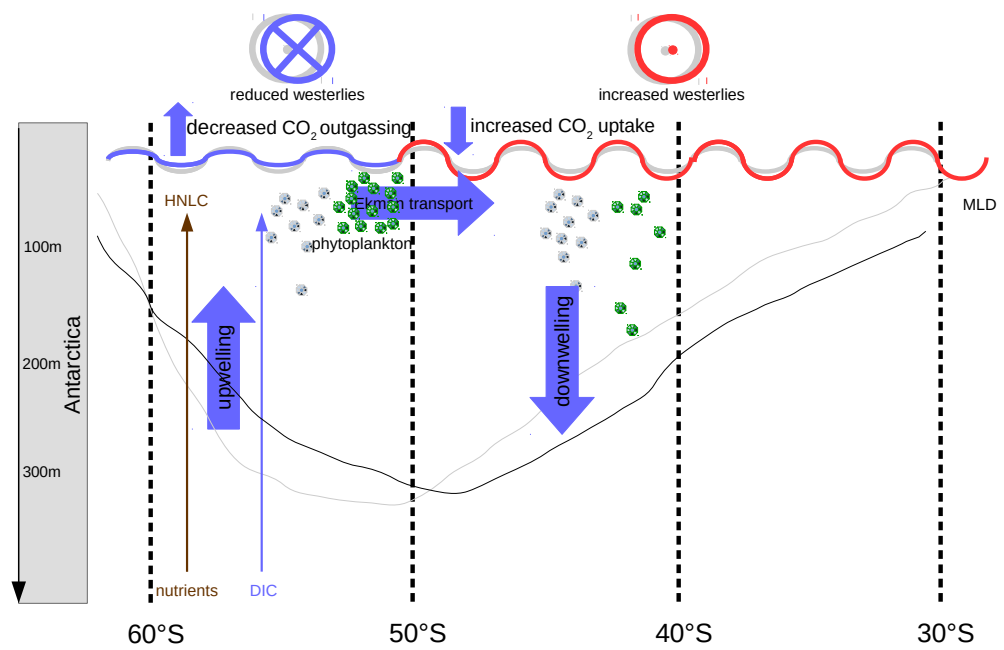


Figure 15: Schematic illustration of the Southern Ocean under the context of decreasing westerly winds

4.2.1 Changes in biology in positive trends

on trends in co2flux, intpp Primary production and CO₂flux show opposing trend patterns as plankton growth takes up less surface DIC and hence pCO₂ increases fig. 14. refer to fig. 16

on explaining intpp increase in 50s: using less zmld mixing refer fig. 17

on intpp not decreasing because of less nutrients different than [Lovenduski and Gruber, 2005] (can I cite this here or only in discussion?)

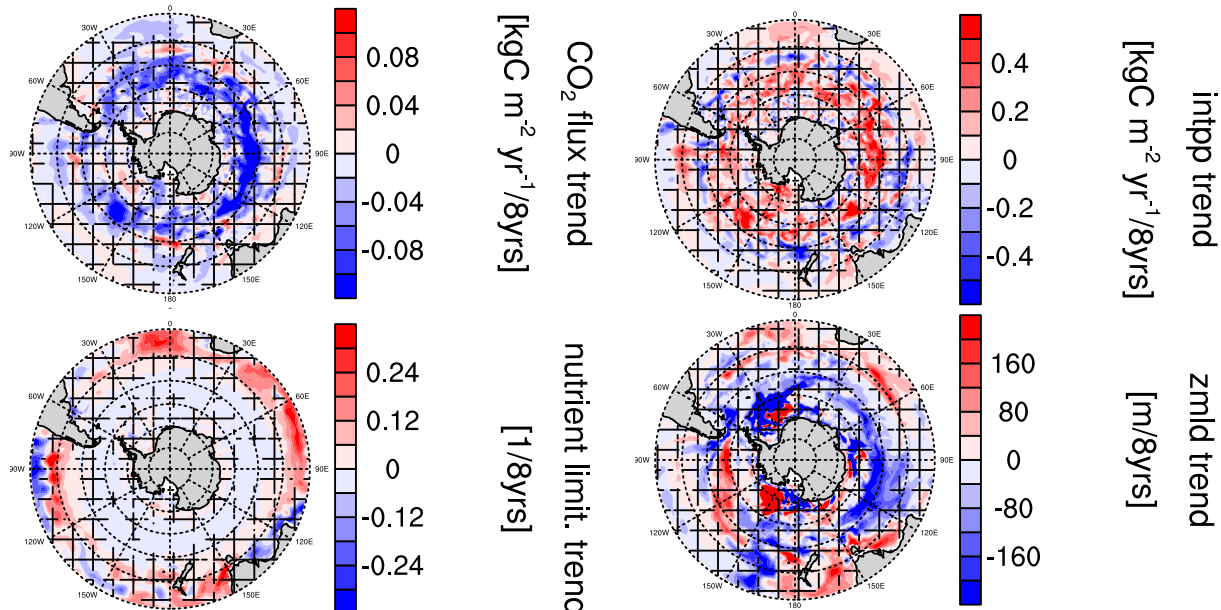


Figure 16: Southern Ocean austral summer trends per per 8 years: CO₂flux (top left), vertically integrated primary production (top right), nutrient limitation (bottom right) and mixed layer depth (bottom left); hatched areas indicate where trends were below 5% significance

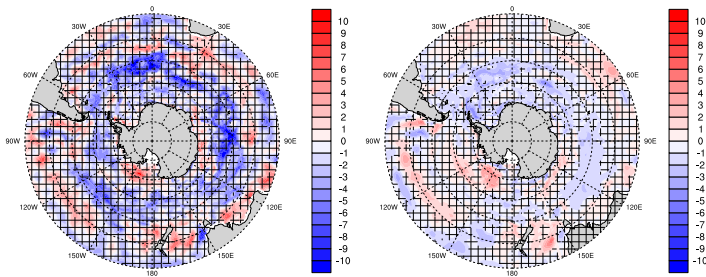


Figure 17: Trends in [m/8yrs] for phytoplankton average depth (left) and average depth of vertical diffusivity due to wind (right); hatched areas indicate where trends were below 5% significance

4.2.2 Changes in ocean circulation in positive trends

transition: zmlt trends; Upper-ocean overturning circulation: up, ekman transport, downwelling The strong stabilizing trend in MLD could also be a sign of decreasing outgassing due to less mixing (fig. 16). refer to fig. 18

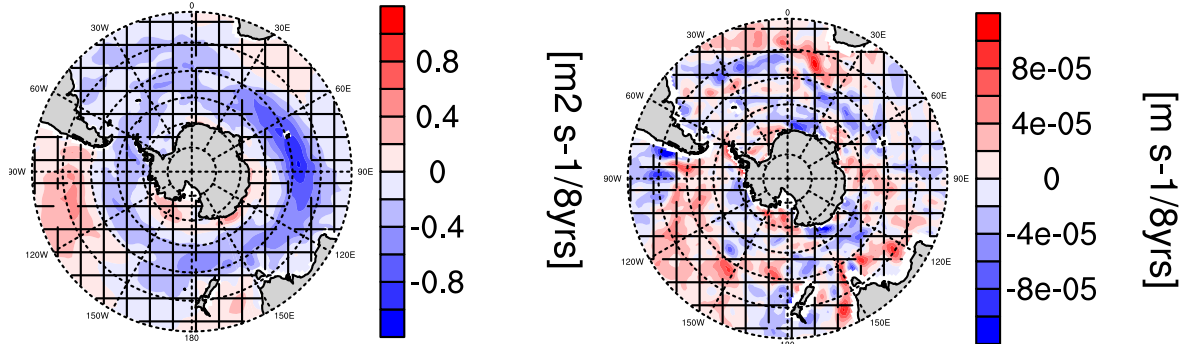


Figure 18: Ekman transport and ekman upwelling trends

carbon transport changes refer fig. 19

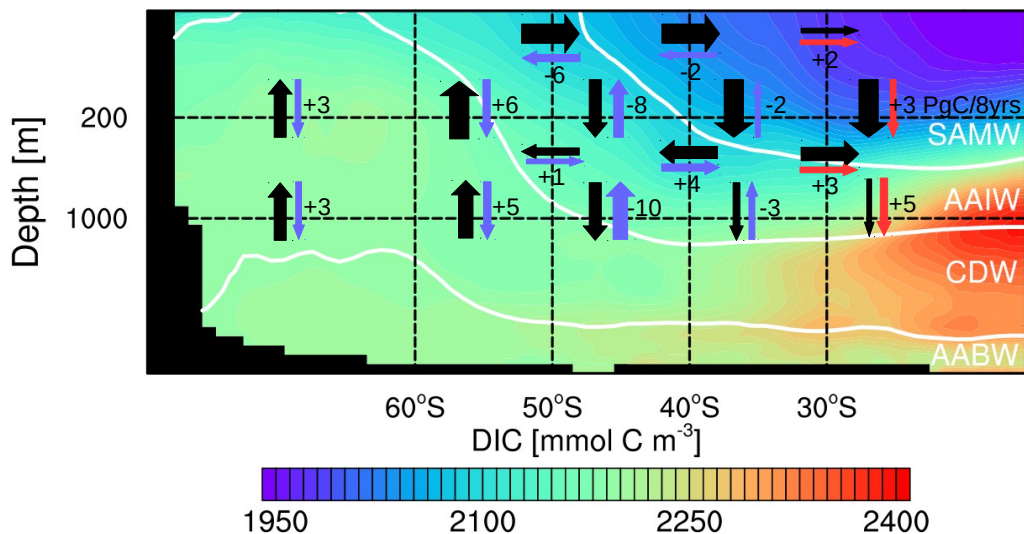


Figure 19: Decreased upper-ocean overturning circulation strengthens the carbon sink as carbon-rich water are less upwelled and carbon-depleted water are less downwelled

4.3 Internal Variability due to winds

on difference regimes, correlation plots co2flux and wind trends fig. 20 refer to fig. 9 and fig. 15

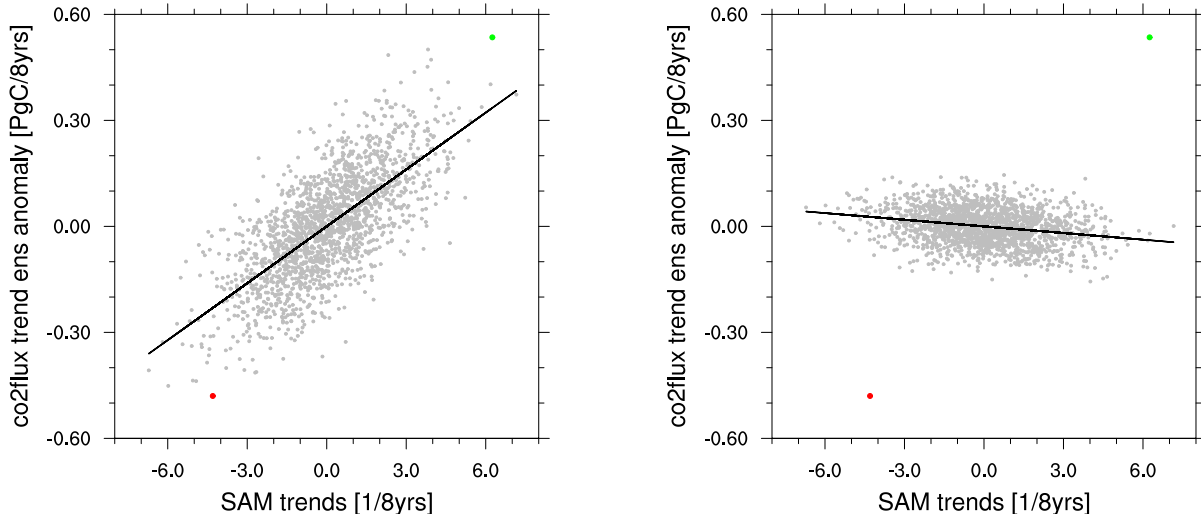


Figure 20: Southern Annular Mode (SAM) as indicator of wind strength vs. CO₂flux south of 35°S; left 50-60s; right 40-50; one data point represents 8-year trends of single realization minus ensemble mean in 8-year periods between 1980 and 2005; red dot is negative trend example, green dot is positive trend example;

5 Discussion

My results in perspective...

on comparison biology paper : Iron-hypothesis [Martin, 1990] doesn't apply to HAMOCC, similar zmlld co2flux response, though location differs [Lovenduski and Gruber, 2005, Hauck et al., 2013, Wang and Moore, 2012]

on comparison circulation paper upwelling found to be major carbon sink driver [Landschützer et al., 2015, Le Quéré et al., 2007, Lovenduski et al., 2007], upwelling location boundaries differ slightly, upwelling trends deeper into ocean [DeVries et al., 2017]

on comparison earlier co2flux paper trend in same order of magnitude reproduced; different 1980s anomaly [Le Quéré et al., 2007, Lovenduski et al., 2007, Landschützer et al., 2015] also reference to Sarmiento ARGO estimates: strength: insitu two years; weakness: few floats for large areas; SOM-FFN 2016 might be seasonally biased; interactive carbon cycle produces 25% higher internal variability [Ilyina et al., 2013]

on internal variability US models have tropical and Indian Pacific as dominating variability mode region, MPI has Southern Ocean, MPI has higher int var than CESM, but lower than GFDL [?]

on ensemble comparisons CESM LE cannot reproduce decadal trends [private communication] weak SO carbon sink [McKinley et al., 2016] or even GFDL [Rodgers et al., 2015]

on MPI-OM SO performance evaluation papers [Jungclaus et al., 2013, Sallée et al., 2013, Salle et al., 2013, Heuzé et al., 2013, Stössel et al., 2015]

on HAMOCC SO performance pCO₂ comparison Takahashi or surface DIC GLO-DAP [Ilyina et al., 2013] or new comparison with Landschützer in Results II? amplified seasonal cycle [Nevison et al., 2016], APO and CO₂ sink [Nevison et al., 2015], early HAMOCC tuned for NH [Six and Maier-Reimer, 1996]

6 Summary and conclusions

what I did and internal variability value ± make sure three questions are answered

two wind regimes of internal variability processes processes at 50-60S linking to wind and summarising results of figure 20

outlook: large ensemble variability modeling Outlook paragraph on internal variability from large ensemble simulations; unlike CESM LE emphasis on HAMOCC SO seasonal cycle?

outlook: focus SO: ARGO data and SOMFFN combined

References and Notes

- M. Bittner, H. Schmidt, C. Timmreck, and F. Sienz. Using a large ensemble of simulations to assess the Northern Hemisphere stratospheric dynamical response to tropical volcanic eruptions and its uncertainty. *Geophysical Research Letters*, 43(17):9324–9332, 2016. ISSN 1944-8007. doi: 10.1002/2016GL070587. URL <http://dx.doi.org/10.1002/2016GL070587>. 2016GL070587.
- C. Deser, A. Phillips, V. Bourdette, and H. Teng. Uncertainty in climate change projections: the role of internal variability. *Clim Dyn*, 38(3-4):527–546, dec 2012. doi: 10.1007/s00382-010-0977-x. URL <http://dx.doi.org/10.1007/s00382-010-0977-x>.
- T. DeVries, M. Holzer, and F. Primeau. Recent increase in oceanic carbon uptake driven by weaker upper-ocean overturning. *Nature*, 542(7640):215–218, feb 2017. doi: 10.1038/nature21068. URL <https://doi.org/10.1038%2Fnature21068>.
- R. W. Eppley. Temperature and phytoplankton growth in the sea. *Fishery Bulletin*, 70(4):1063–1085, 1972.
- P. J. S. Franks. Has sverdrup’s critical depth hypothesis been tested? mixed layers vs. turbulent layers. *ICES Journal of Marine Science: Journal du Conseil*, 72(6):1897–1907, oct 2014. doi: 10.1093/icesjms/fsu175.
- M. A. Giorgetta, J. Jungclaus, C. H. Reick, S. Legutke, J. Bader, M. Böttinger, V. Brovkin, T. Crueger, M. Esch, K. Fieg, K. Glushak, V. Gayler, H. Haak, H.-D. Hollweg, T. Ilyina, S. Kinne, L. Kornblueh, D. Matei, T. Mauritzen, U. Mikolajewicz, W. Mueller, D. Notz, F. Pithan, T. Raddatz, S. Rast, R. Redler, E. Roeckner, H. Schmidt, R. Schnur, J. Segschneider, K. D. Six, M. Stockhausen, C. Timmreck, J. Wegner, H. Widmann, K.-H. Wieners, M. Claussen, J. Marotzke, and B. Stevens. Climate and carbon cycle changes from 1850 to 2100 in mpi-esm simulations for the coupled model intercomparison project phase 5. *Journal of Advances in Modeling Earth Systems*, 5(3):572–597, 2013. ISSN 1942-2466. doi: 10.1002/jame.20038. URL <http://dx.doi.org/10.1002/jame.20038>.
- J. Hauck, C. Völker, T. Wang, M. Hoppema, M. Losch, and D. A. Wolf-Gladrow. Seasonally different carbon flux changes in the southern ocean in response to the south-

- ern annular mode. *Global Biogeochemical Cycles*, 27(4):1236–1245, dec 2013. doi: 10.1002/2013gb004600. URL <http://dx.doi.org/10.1002/2013GB004600>.
- C. Heinze, E. Maier-Reimer, and K. Winn. Glacial pco₂ reduction by the world ocean: Experiments with the hamburg carbon cycle model. *Paleoceanography*, 6(4):395–430, 1991. ISSN 1944-9186. doi: 10.1029/91PA00489. URL <http://dx.doi.org/10.1029/91PA00489>.
- C. Heuzé, K. J. Heywood, D. P. Stevens, and J. K. Ridley. Southern ocean bottom water characteristics in CMIP5 models. *Geophys. Res. Lett.*, 40(7):1409–1414, apr 2013. doi: 10.1002/grl.50287. URL <http://dx.doi.org/10.1002/grl.50287>.
- T. Ilyina, K. D. Six, J. Segschneider, E. Maier-Reimer, H. Li, and I. Núñez-Riboni. Global ocean biogeochemistry model hamocc: Model architecture and performance as component of the mpi-earth system model in different cmip5 experimental realizations. *Journal of Advances in Modeling Earth Systems*, 5(2):287–315, 2013. ISSN 1942-2466. doi: 10.1029/2012MS000178. URL <http://dx.doi.org/10.1029/2012MS000178>.
- J. H. Jungclaus, N. Fischer, H. Haak, K. Lohmann, J. Marotzke, D. Matei, U. Mikolajewicz, D. Notz, and J. S. von Storch. Characteristics of the ocean simulations in the max planck institute ocean model (mpiom) the ocean component of the mpi-earth system model. *Journal of Advances in Modeling Earth Systems*, 5(2):422–446, 2013. ISSN 1942-2466. doi: 10.1002/jame.20023. URL <http://dx.doi.org/10.1002/jame.20023>.
- J. E. Kay, C. Deser, A. Phillips, A. Mai, C. Hannay, G. Strand, J. M. Arblaster, S. C. Bates, G. Danabasoglu, J. Edwards, M. Holland, P. Kushner, J.-F. Lamarque, D. Lawrence, K. Lindsay, A. Middleton, E. Munoz, R. Neale, K. Oleson, L. Polvani, and M. Vertenstein. The community earth system model (CESM) large ensemble project: A community resource for studying climate change in the presence of internal climate variability. *Bull. Amer. Meteor. Soc.*, 96(8):1333–1349, aug 2015. doi: 10.1175/bams-d-13-00255.1. URL <http://dx.doi.org/10.1175/BAMS-D-13-00255.1>.
- P. Landschützer, N. Gruber, F. A. Haumann, C. Rödenbeck, D. C. E. Bakker, S. van Heuven, M. Hoppema, N. Metzl, C. Sweeney, T. Takahashi, B. Tilbrook, and R. Wanninkhof. The reinvigoration of the southern ocean carbon sink. *Science*, 349(6253):

1221–1224, 2015. ISSN 0036-8075. doi: 10.1126/science.aab2620. URL <http://science.sciencemag.org/content/349/6253/1221>.

P. Landschtzer, N. Gruber, D. C. E. Bakker, and U. Schuster. Recent variability of the global ocean carbon sink. *Global Biogeochemical Cycles*, 28(9):927–949, sep 2014. doi: 10.1002/2014gb004853. URL <http://dx.doi.org/10.1002/2014GB004853>.

P. Landschtzer, N. Gruber, and D. C. E. Bakker. Decadal variations and trends of the global ocean carbon sink. *Global Biogeochemical Cycles*, 30(10):1396–1417, oct 2016. doi: 10.1002/2015gb005359. URL <https://doi.org/10.1002%2F2015gb005359>.

C. Le Quéré, C. Rödenbeck, E. T. Buitenhuis, T. J. Conway, R. Langenfelds, A. Gomez, C. Labuschagne, M. Ramonet, T. Nakazawa, N. Metzl, N. Gillett, and M. Heimann. Saturation of the southern ocean co₂ sink due to recent climate change. *Science*, 316 (5832):1735–1738, 2007. ISSN 0036-8075. doi: 10.1126/science.1136188. URL <http://science.sciencemag.org/content/316/5832/1735>.

C. Le Quéré, R. M. Andrew, J. G. Canadell, S. Sitch, J. I. Korsbakken, G. P. Peters, A. C. Manning, T. A. Boden, P. P. Tans, R. A. Houghton, R. F. Keeling, S. Alin, O. D. Andrews, P. Anthoni, L. Barbero, L. Bopp, F. Chevallier, L. P. Chini, P. Ciais, K. Currie, C. Delire, S. C. Doney, P. Friedlingstein, T. Gkritzalis, I. Harris, J. Hauck, V. Haverd, M. Hoppema, K. K. Goldewijk, A. K. Jain, E. Kato, A. Körtzinger, P. Landschützer, N. Lefèvre, A. Lenton, S. Lienert, D. Lombardozzi, J. R. Melton, N. Metzl, F. Millero, P. M. S. Monteiro, D. R. Munro, J. E. M. S. Nabel, S. Nakaoka, K. O'Brien, A. Olsen, A. M. Omar, T. Ono, D. Pierrot, B. Poulter, C. Rödenbeck, J. Salisbury, U. Schuster, J. Schwinger, R. Séférian, I. Skjelvan, B. D. Stocker, A. J. Sutton, T. Takahashi, H. Tian, B. Tilbrook, I. T. van der Laan-Luijkx, G. R. van der Werf, N. Viovy, A. P. Walker, A. J. Wiltshire, and S. Zaehle. Global carbon budget 2016. *Earth System Science Data*, 8(2):605–649, nov 2016. doi: 10.5194/essd-8-605-2016. URL <http://dx.doi.org/10.5194/essd-8-605-2016>.

N. S. Lovenduski and N. Gruber. Impact of the southern annular mode on southern ocean circulation and biology. *Geophys. Res. Lett.*, 32(L11603), 2005. doi: 10.1029/2005GL022727. URL <http://onlinelibrary.wiley.com/doi/10.1029/2005GL022727/pdf>.

- N. S. Lovenduski, N. Gruber, S. C. Doney, and I. D. Lima. Enhanced co₂ outgassing in the southern ocean from a positive phase of the southern annular mode. *Global Biogeochemical Cycles*, 21(2):n/a–n/a, 2007. ISSN 1944-9224. doi: 10.1029/2006GB002900. URL <http://dx.doi.org/10.1029/2006GB002900>. GB2026.
- N. S. Lovenduski, G. A. McKinley, A. R. Fay, K. Lindsay, and M. C. Long. Partitioning uncertainty in ocean carbon uptake projections: Internal variability, emission scenario, and model structure. *Global Biogeochemical Cycles*, 30(9):1276–1287, sep 2016. doi: 10.1002/2016gb005426. URL <http://dx.doi.org/10.1002/2016GB005426>.
- J. Marotzke and P. M. Forster. Forcing, feedback and internal variability in global temperature trends. *Nature*, 517(7536):565–570, jan 2015. doi: 10.1038/nature14117. URL <http://dx.doi.org/10.1038/nature14117>.
- J. Marshall and K. Speer. Closure of the meridional overturning circulation through southern ocean upwelling. *Nature Geoscience*, 5(3):171–180, feb 2012. doi: 10.1038/ngeo1391. URL <http://dx.doi.org/10.1038/NGE01391>.
- J. H. Martin. Glacial-interglacial CO₂ change: The Iron Hypothesis. *Paleoceanography*, 5(1):1–13, 1990. ISSN 1944-9186. doi: 10.1029/PA005i001p00001. URL <http://dx.doi.org/10.1029/PA005i001p00001>.
- G. A. McKinley, D. J. Pilcher, A. R. Fay, K. Lindsay, M. C. Long, and N. S. Lovenduski. Timescales for detection of trends in the ocean carbon sink. *Nature*, 530(7591):469–472, feb 2016. doi: 10.1038/nature16958. URL <http://dx.doi.org/10.1038/nature16958>.
- C. D. Nevison, M. Manizza, R. F. Keeling, M. Kahru, L. Bopp, J. Dunne, J. Tiputra, T. Ilyina, and B. G. Mitchell. Evaluating the ocean biogeochemical components of earth system models using atmospheric potential oxygen and ocean color data. *Biogeosciences*, 12(1):193–208, jan 2015. doi: 10.5194/bg-12-193-2015. URL <http://dx.doi.org/10.5194/bg-12-193-2015>.
- C. D. Nevison, M. Manizza, R. F. Keeling, B. B. Stephens, J. D. Bent, J. Dunne, T. Ilyina, M. Long, L. Resplandy, J. Tjiputra, and S. Yukimoto. Evaluating CMIP5 ocean biogeochemistry and southern ocean carbon uptake using atmospheric potential oxygen: Present-day performance and future projection. *Geophys. Res. Lett.*, 43

(5):2077–2085, mar 2016. doi: 10.1002/2015gl067584. URL <http://dx.doi.org/10.1002/2015GL067584>.

K. B. Rodgers, J. Lin, and T. L. Frlicher. Emergence of multiple ocean ecosystem drivers in a large ensemble suite with an earth system model. *Biogeosciences*, 12(11):3301–3320, jun 2015. doi: 10.5194/bg-12-3301-2015. URL <https://doi.org/10.5194%2Fbg-12-3301-2015>.

C. L. Sabine, R. A. Feely, N. Gruber, R. M. Key, K. Lee, J. L. Bullister, R. Wanninkhof, C. S. Wong, D. W. R. Wallace, B. Tilbrook, F. J. Millero, T.-H. Peng, A. Kozyr, T. Ono, and A. F. Rios. The oceanic sink for anthropogenic co₂. *Science*, 305(5682):367–371, 2004. ISSN 0036-8075. doi: 10.1126/science.1097403. URL <http://science.scienmag.org/content/305/5682/367>.

J.-B. Sallée, E. Shuckburgh, N. Bruneau, A. J. S. Meijers, T. J. Bracegirdle, and Z. Wang. Assessment of southern ocean mixed-layer depths in CMIP5 models: Historical bias and forcing response. *J. Geophys. Res. Oceans*, 118(4):1845–1862, apr 2013. doi: 10.1002/jgrc.20157. URL <http://dx.doi.org/10.1002/jgrc.20157>.

J.-B. Salle, E. Shuckburgh, N. Bruneau, A. J. S. Meijers, T. J. Bracegirdle, Z. Wang, and T. Roy. Assessment of southern ocean water mass circulation and characteristics in cmip5 models: Historical bias and forcing response. *Journal of Geophysical Research: Oceans*, 118(4):1830–1844, 2013. ISSN 2169-9291. doi: 10.1002/jgrc.20135. URL <http://dx.doi.org/10.1002/jgrc.20135>.

K. D. Six and E. Maier-Reimer. Effects of plankton dynamics on seasonal carbon fluxes in an ocean general circulation model. *Global Biogeochemical Cycles*, 10(4):559–583, 1996. ISSN 1944-9224. doi: 10.1029/96GB02561. URL <http://dx.doi.org/10.1029/96GB02561>.

B. Stevens, M. Giorgetta, M. Esch, T. Mauritsen, T. Crueger, S. Rast, M. Salzmann, H. Schmidt, J. Bader, K. Block, R. Brokopf, I. Fast, S. Kinne, L. Kornblueh, U. Lohmann, R. Pincus, T. Reichler, and E. Roeckner. Atmospheric component of the MPI-M Earth System Model: ECHAM6. *Journal of Advances in Modeling Earth Systems*, 5(2):146–172, 2013. ISSN 1942-2466. doi: 10.1002/jame.20015. URL <http://dx.doi.org/10.1002/jame.20015>.

- A. Stössel, D. Notz, F. A. Haumann, H. Haak, J. Jungclaus, and U. Mikolajewicz. Controlling high-latitude southern ocean convection in climate models. *Ocean Modelling*, 86: 58 – 75, 2015. ISSN 1463-5003. doi: <http://dx.doi.org/10.1016/j.ocemod.2014.11.008>. URL <http://www.sciencedirect.com/science/article/pii/S1463500314001760>.
- H. U. Sverdrup. On conditions for the vernal blooming of phytoplankton. *Journal du Conseil International pour l'Exploration de la Mer*, 18:287–295, 1953.
- K. E. Taylor, R. J. Stouffer, and G. A. Meehl. An overview of CMIP5 and the experiment design. *Bull. Amer. Meteor. Soc.*, 93(4):485–498, apr 2012. doi: 10.1175/bams-d-11-00094.1. URL <http://dx.doi.org/10.1175/BAMS-D-11-00094.1>.
- D. W. J. Thompson, E. A. Barnes, C. Deser, W. E. Foust, and A. S. Phillips. Quantifying the role of internal climate variability in future climate trends. *Journal of Climate*, 28 (16):6443–6456, aug 2015. doi: 10.1175/jcli-d-14-00830.1. URL <http://dx.doi.org/10.1175/JCLI-D-14-00830.1>.
- S. Wang and J. K. Moore. Variability of primary production and air-sea CO₂ flux in the Southern Ocean. *Global Biogeochemical Cycles*, 26(1):n/an/a, 2012. ISSN 1944-9224. doi: 10.1029/2010GB003981. URL <http://dx.doi.org/10.1029/2010GB003981>. GB1008.
- R. Wanninkhof. Relationship between wind speed and gas exchange over the ocean. *Journal of Geophysical Research: Oceans*, 97(C5):7373–7382, 1992. ISSN 2156-2202. doi: 10.1029/92JC00188. URL <http://dx.doi.org/10.1029/92JC00188>.

List of Figures

1	Schematic illustration of the Southern Ocean ; probably wrong location here, but where to put it? Results I after the mean state results?	2
2	Schematic overview on the different components in MPI-Earth-System-Model with a diagnostic carbon cycle [Giorgetta et al., 2013]	4
3	A schematic overview of the global ocean biogeochemistry model HAMOCC [Ilyina et al., 2013]	5
4	Evolution of the Southern Ocean carbon sink anomaly south of 35°S. Grey lines show the 100 ensemble members, the black line the ensemble median, the gray shading is the range of the ensemble, the blue shading is the 1σ ensemble spread, the red lines are decreasing sink trend candidates, the blue line is the SOM-FFN observation-based estimate; negative values indicate anomalous uptake with respect to the 1980s	7
5	Evolution of the Southern Ocean primary production south of 35°S. Grey lines show the 100 ensemble members, the black line the ensemble median, the gray shading is the range of the ensemble, the blue shading is the 2σ ensemble spread, the red lines are decreasing sink trend candidates	8
6	Spatial distribution of the yearmean Southern Ocean CO ₂ flux (top) and primary production (bottom): negative values indicate ocean uptake ensemble median (left) as forced signal and ensemble standard deviation (right) as internal variability	9
7	Upper-ocean overturning circulation modulates the carbon sink as carbon-rich water are upwelled and carbon-depleted water are downwelled; black arrows show yearly mean advective carbon transport; white lines are isopyncals separating Sub-Antarctic Mode Water (SAMW), Antarctic Intermediate Water (AAIW), Circumpolar Deep Water (CDW) and Antarctic Bottom Water (AABW)	10
8	pCO ₂ (right) (left) and Trends in sea-level pressure and winds	11
9	Schematic illustration of the Southern Ocean under the context of increasing westerly winds and response of biology and upper-ocean circulation towards the carbon sink	11
10	Southern Ocean austral summer trends per 8 years	12

11	Trends in [m/8yrs] for phytoplankton average depth (left) and average depth of vertical diffusivity due to wind (right); hatched areas indicate where trends were below 5% significance	13
12	Ekman transport and ekman upwelling trends	14
13	Increased upper-ocean overturning circulation weakens the carbon sink as carbon-rich water are upwelled and carbon-depleted water are downwelled .	14
14	Trends in pCO ₂ (left) and sea-level pressure and winds (right)	15
15	Schematic illustration of the Southern Ocean under the context of decreasing westerly winds	16
16	Southern Ocean austral summer trends per 8 years: CO ₂ flux (top left), vertically integrated primary production (top right), nutrient limitation (bottom right) and mixed layer depth (bottom left); hatched areas indicate where trends were below 5% significance	17
17	Trends in [m/8yrs] for phytoplankton average depth (left) and average depth of vertical diffusivity due to wind (right); hatched areas indicate where trends were below 5% significance	18
18	Ekman transport and ekman upwelling trends	19
19	Decreased upper-ocean overturning circulation strengthens the carbon sink as carbon-rich water are less upwelled and carbon-depleted water are less downwelled	19
20	Southern Annular Mode (SAM) as indicator of wind strength vs. CO ₂ flux south of 35°S; left 50-60s; right 40-50; one data point represents 8-year trends of single realization minus ensemble mean in 8-year periods between 1980 and 2005; red dot is negative trend example, green dot is positive trend example;	20
21	Southern Ocean carbon sink: yearmean fieldsum 35-90S (left) and yearmean in a random grid cell (right)	31
22	Southern Ocean carbon sink trends per trendlength; (above) normal; (below) detrended from ensmean trend	32

Supplementary information

Statistics of Southern Ocean carbon sink

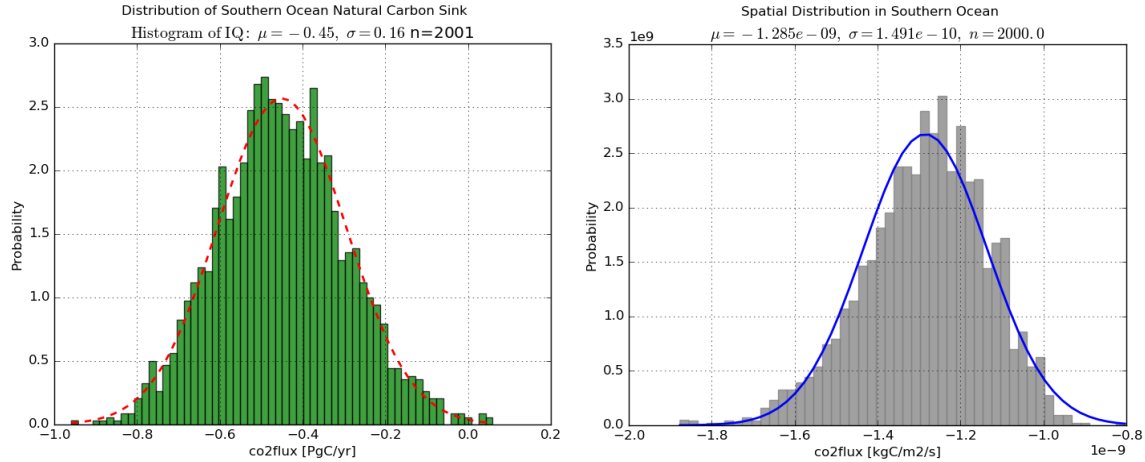


Figure 21: Southern Ocean carbon sink: yearmean fieldsum 35-90S (left) and yearmean in a random grid cell (right)

CO₂flux trends heatmap in MPI-ESM Large Ensemble

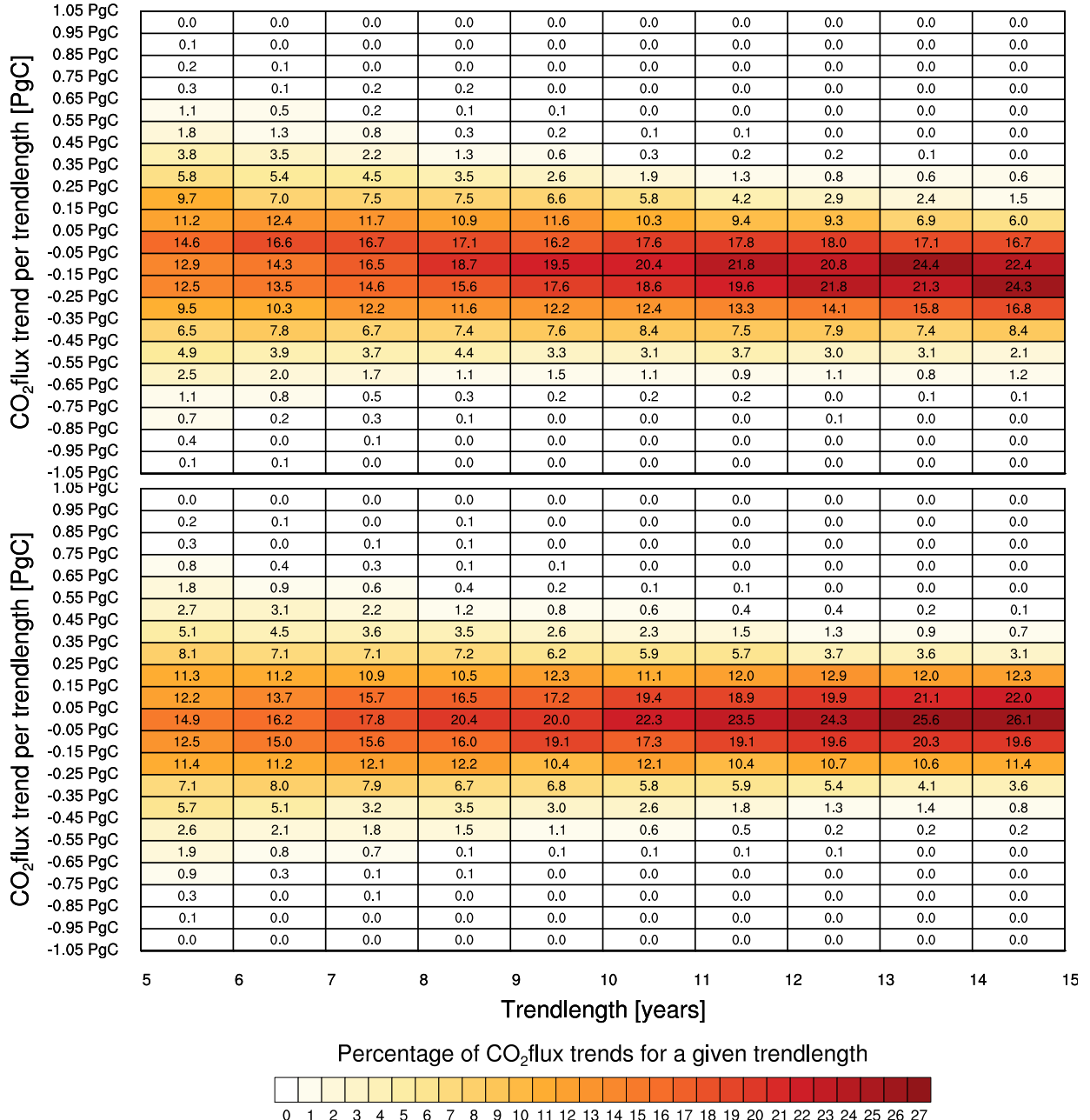


Figure 22: Southern Ocean carbon sink trends per trendlength; (above) normal; (below) detrended from ensmean trend